

1. Acoustic Pressure Response Computations using Modal Analysis.

This paper presents the computation of Acoustic Pressure Responses (APRs) for the considered 1D periodic acoustic metamaterials. The main objectives are twofold: firstly, to demonstrate the validity of FE-Bloch's theorem by comparing frequencies corresponding to attenuated regions in the APRs with computed bandgap frequencies dependent on the FE-Bloch's theorem unit cell; and secondly, to evaluate and analyze the sound-attenuation performance of the entire 1D periodic acoustic metamaterial through obtained Acoustic Sound Pressure Level computations.

To achieve these objectives, this work employs a modal analysis approach for computing the acoustic pressure response of the 1D acoustic metamaterial. The Modal Analysis technique is commonly used in the field of harmonics to study the modal contributions and frequency response. This approach was chosen for its computational efficiency. In this study, a combination of modal analysis principles and finite element method is employed to accurately calculate the acoustic pressure response. Initially, the eigenvalue Problem of 1D periodic metamaterials consisting of tessellated unit cells connected by lattice vectors (\mathbf{e}) is solved using ABAQUS software package. The corresponding eigenfrequencies and eigenvectors are determined using LANSOZ SOLVER. These eigenfrequencies and eigenvectors are then utilized in Modal Analysis to compute the acoustic pressure responses. Modal Analysis assumes the acoustic pressure response to be a sum of modal contributions, where each mode is characterized by a specific frequency and associated vibration pattern.

$$P = [P_m][q] \quad (\text{S.1})$$

Equation (S.1) depicts the expression for the acoustic pressure as a summation of the eigenvectors and their respective contributions through modal acoustic pressure. Where (P_m) is the eigenvectors that are normalized by the mass matrix, while the modal acoustic pressure is denoted by (q). To compute the modal acoustic pressures (q), decoupled time-dependent ordinary differential equations are utilized.

$$\ddot{q}_{ii} + \omega_{ii}^2 q_{ii} = [P_m]^T [f(t)] \quad (\text{S.2})$$

The decoupled time-dependent ordinary differential equation in the modal coordinates is represented by Equation (S.2), where ω corresponds to the eigenfrequencies of the modes and i denotes to the mode number. The force vector $f(t)$ represents an external sound source that excites the system. The transform function of Equation (S.2) will be used to compute the acoustic pressure responses.

$$S^2 Q_{ii}(S) + \omega_{ii}^2 Q_{ii}(S) = [P_m]^T [F(S)] \quad (\text{S.3})$$

Equation (S.3) represents the transfer function of Equation (S.2). This transfer function allows for the transformation of the ordinary differential equation from the time domain to the frequency domain (i.e., S domain). By rewriting Equation (S.3), it can be directly used to calculate modal acoustic pressure in the frequency domain.

$$Q(s) = (I(S^2 + \omega^2))^{-1} [P_m]^T [F(S)] \quad (\text{S.4})$$

Equation (S.4) represents a revised form of Equation (S.3) that facilitates the calculation of modal acoustic pressure in the frequency domain. In turn, Equation (S.1) is employed to solve for the acoustic pressure in this domain. It should be emphasized that an impulse signal is assumed as the external sound source that will stimulate the system. Further details regarding this assumption is discussed in sections showing the acoustic pressure response results.

2. Bandgaps' Key-Features

In this study, important characteristics were taken into account to summarize the multiple bandgap data acquired in the preceding subsection and also serve as key indicators of performance for the designs under consideration. Two significant features relating to bandgaps were examined: the Size of the Widest bandgap and the Centroid of the Widest Bandgap. These particular properties were originally introduced by *Shendy et al.* [1], serving as concise descriptors that capture essential information about how bandgaps behave in metamaterials. This study will analyze the normalized size and centroid of the widest bandgap in accordance with the data on bandgaps. The consideration of bandgap key-features in this work is crucial for summarizing the extensive data on bandgaps obtained in the previous subsection and also will play a role in the filtering step along with the obtained bandgaps data.

$$S.O.W.B = \frac{\Delta f C}{c} \quad (S.5)$$

According to Equation (S.5), the normalized Size of the Widest Bandgap (*S.O.W.B*) can be determined. In this equation, (Δf) represents the actual Size of the Widest Bandgap, (*C*) is the unit cell size, and (*c*) denotes the speed of sound in air medium. The equation suggests that as the unit cell size increases, there is a decrease in the actual Size of the Widest Bandgap.

$$C.O.W.B = \frac{f_c C}{c} \quad (S.6)$$

While Equation (S.6) represents the normalized Centroid of the Widest Bandgap (*C.O.W.B*). (f_c) represents the actual Centroid of the Widest Bandgap. Similar to the inversely proportional relation between the normalized Size of the Widest Bandgap and unit cell size, it's also observed that the normalized Centroid of the Widest Bandgap decreases as the unit cell size increases. Both key-features allows for the comparison of bandgap characteristics across different designs and provides valuable insights into the performance of each design in terms of frequency range and localization. It is important to note that the widest bandgap occurs at the first acoustic bandgap in all types of unit cells (i.e., Basic-Periodic unit cells, Semi-Periodic unit cells, Tapered-Diverging unit cells, and Tapered-Converging unit cells). As the size of the unit cell increases, this first bandgap occurs at lower frequency ranges. However, it should be noted that while this may be advantageous in blocking audible frequencies, both the size of the first bandgap and other subsequent bandgaps will become smaller.

Both Figure S 1 and Figure S 2 depict the key features considered in this study, namely the variations in bandgap width and centroid for different design configurations (i.e., Basic-Periodic unit cells, Semi-Periodic unit cells, Tapered-Diverging unit cells, and Tapered-Converging unit cells). It was observed that the normalized Size of the Widest Bandgap increases as the holes'

diameter decreases through decreasing (d/C) values in the Basic-Periodic designs with fixed (L/C) values and decreasing (d_1/C) and (d_2/d_1) values in the Semi-Periodic, Tapered-Diverging and Tapered-Converging designs with fixed (L/C) values. On the other hand, analyzing the normalized Centroid of the Widest Bandgap in all the designs within the considered design configurations led to two general conclusions. The first general conclusion finding indicated that designs with lower (L/C) values experienced a reduction in the normalized Centroid of the Widest Bandgap as the (d/C) decreases in the Basic-Periodic designs and (d_1/C) decreases in the Semi-Periodic, Tapered-Diverging, and Tapered-Converging designs while maintaining fixed (d_2/d_1) . While, the second general conclusion indicated that designs with higher (L/C) values had the normalized Centroid of the Widest bandgap slightly decreasing or remaining relatively constant as the (d/C) increases in the Basic-Periodic designs and (d_1/C) increases in the Semi-Periodic, Tapered-Diverging and Tapered-Converging designs while maintaining fixed (d_2/d_1) value.

Based on an initial analysis of the key features data, it is anticipated that the optimal design combinations would be those with larger sizes of wide bandgaps in the lower frequency range, achieved by having a lower centroid position and larger size of the widest bandgap. However, these designs occur at small values of (d/C) for Basic-Periodic unit cells and (d_1/C) for Semi-Periodic, Tapered-Diverging and Tapered-Converging unit cells. This results in smaller actual diameter sizes when setting the unit cell size. Complications associated with narrow cylindrical holes being close to boundary layer thicknesses (i.e., visco-thermal boundary layers), Equation 1 may not be applicable and accounting for these layers becomes computationally expensive. Therefore, during the filtering process, designs with diameters significantly larger than their corresponding boundary layers will be considered instead. This is further elaborated in the discussion section.

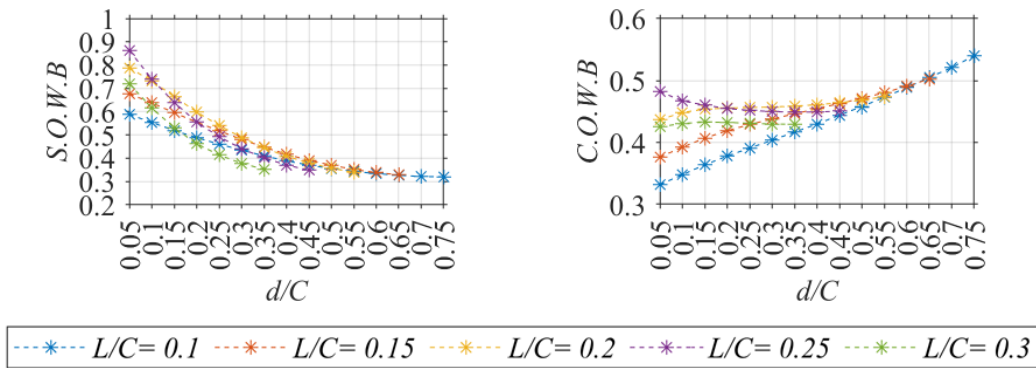


Figure S 1. The normalized Size of the Widest Bandgap (S. O. W. B) and the normalized Centroid of the Widest Bandgap (C. O. W. B) for the considered designs combinations sharing Basic-Periodic unit cell type.

$L/C = 0.1$ $L/C = 0.15$ $L/C = 0.2$ $L/C = 0.25$ $L/C = 0.3$

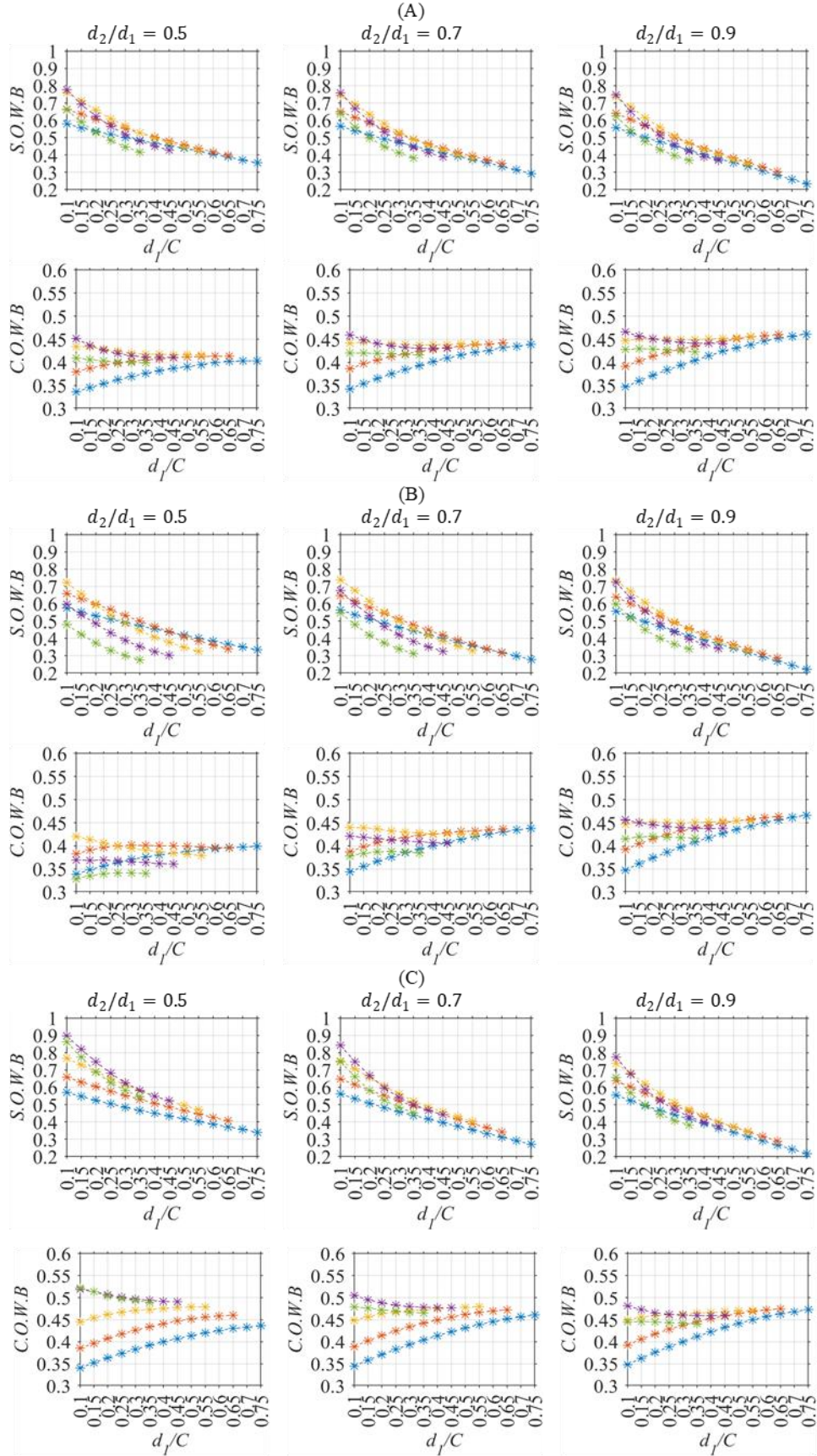


Figure S 2. The normalized Size of the Widest Bandgap (S. O. W. B) and the normalized Centroid of the Widest Bandgap (C. O. W. B) for the considered designs combinations in the geometrically modified unit cell types. A) Semi-Periodic. B) Tapered-Diverging. C) Tapered-Converging.

3. The Relation Between the Unit Cell Size and the Wavelength.

It is crucial to examine the relationship between the size of the unit cell and the acoustic wavelength to understand its impact on bandgap formation. This investigation is prompted by two key physical phenomena observed in metamaterials. The first phenomenon, known as Bragg-Scattering, occurs when the incident wave's wavelength aligns with or is close to that of a unit cell, resulting in destructive interference and subsequent bandgap creation [2,3]. The second phenomenon, called Local Resonance, occurs when a metamaterial attenuates waves with wavelengths significantly larger than its periodicity [4]. To overcome the issue of attenuating lower frequency acoustic waves, Bragg-Scattering requires metamaterials with large unit cell sizes that may be impractical for applications and manufacturing [5]. However, Local Resonance offers a solution by allowing for smaller unit cell sizes to achieve attenuation in lower frequency ranges. The goal of metamaterial research is to develop materials that can effectively attenuate frequencies below the lower limit imposed by Bragg-Scattering. Table S 1 presents a comparison of the unit cell size to wavelength ratio (C/λ_l) between the optimal design in this study and a similar design investigated by *Bilal et al.* [6]. The analysis focuses on the lower-bound wavelength of the first acoustic bandgap (λ_l), as these metamaterials are intended to operate within that range. As demonstrated in Table S 1, our optimal Semi-Periodic unit cell design achieves the lowest unit size to wavelength ratio, indicating superior Local Resonance capabilities compared to other designs. This allows for effective bandgap formation at lower frequency ranges.

Metamaterial	C/λ_l
Optimal Basic-Periodic	0.08
Optimal Semi-Periodic	0.05
Optimal Tapered-Diverging	0.08
Optimal Tapered-Converging	0.07
<i>Bilal et al.</i> [6]	0.18

Table S 1. Unit cell size to wavelength ratio for the considered designs in this comparative study.

4. Acoustic Pressure Response in 1D Periodic Acoustic Metamaterial.

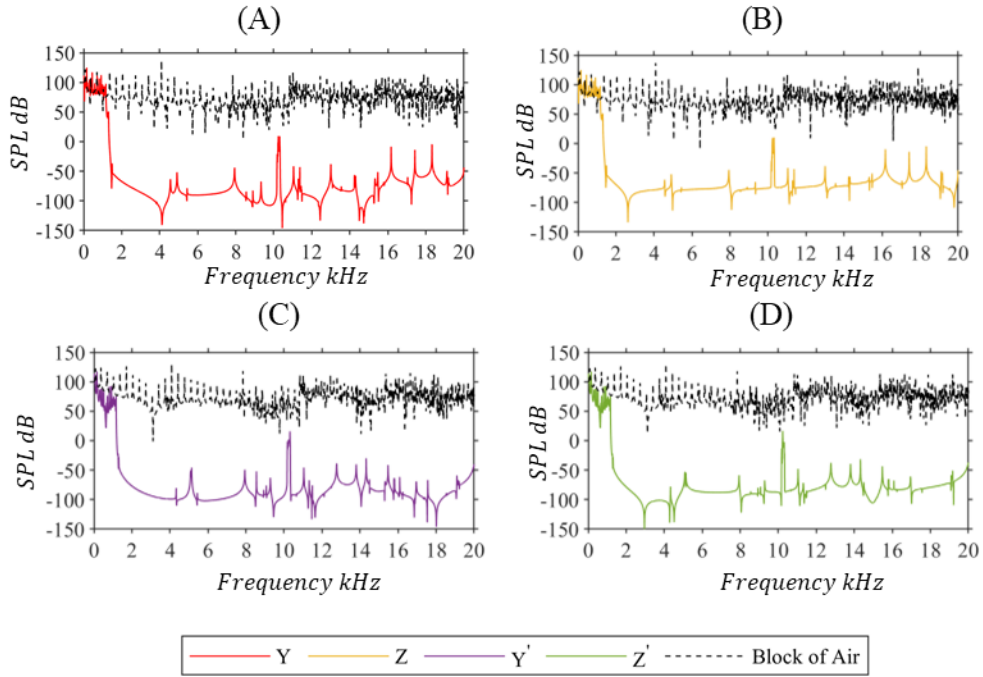


Figure S 3. The acoustic pressure of the other considered sensing locations (i.e., Y,Z,Y',Z') for the 1D acoustic metamaterial made from repeated optimal Basic-Periodic unit cell.

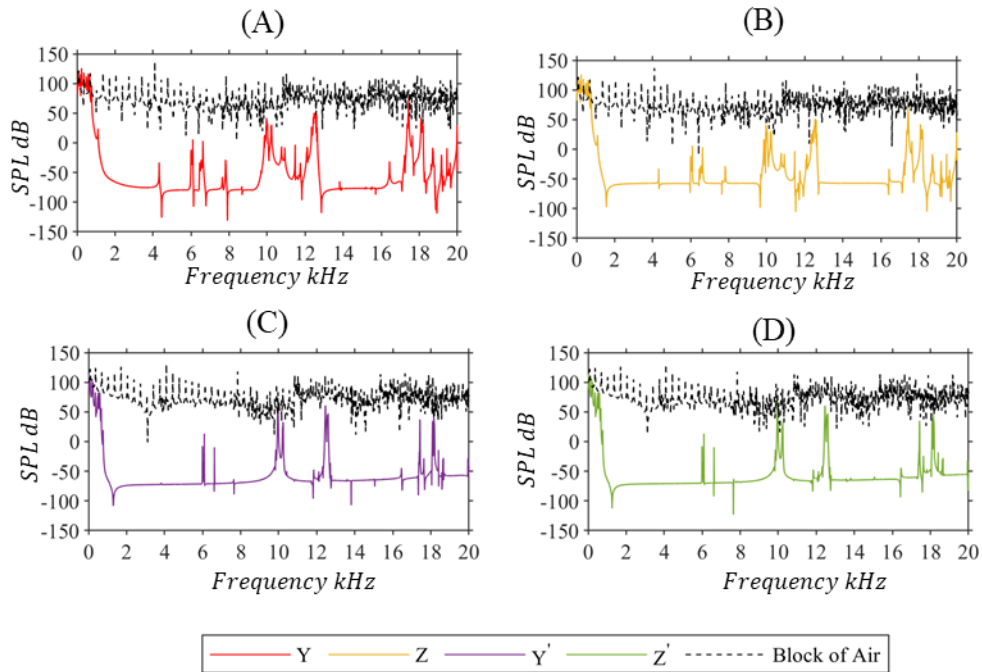


Figure S 4. The acoustic pressure of the other considered sensing locations (i.e., Y,Z,Y',Z') for the 1D acoustic metamaterial made from repeated optimal Semi-Periodic unit cell.

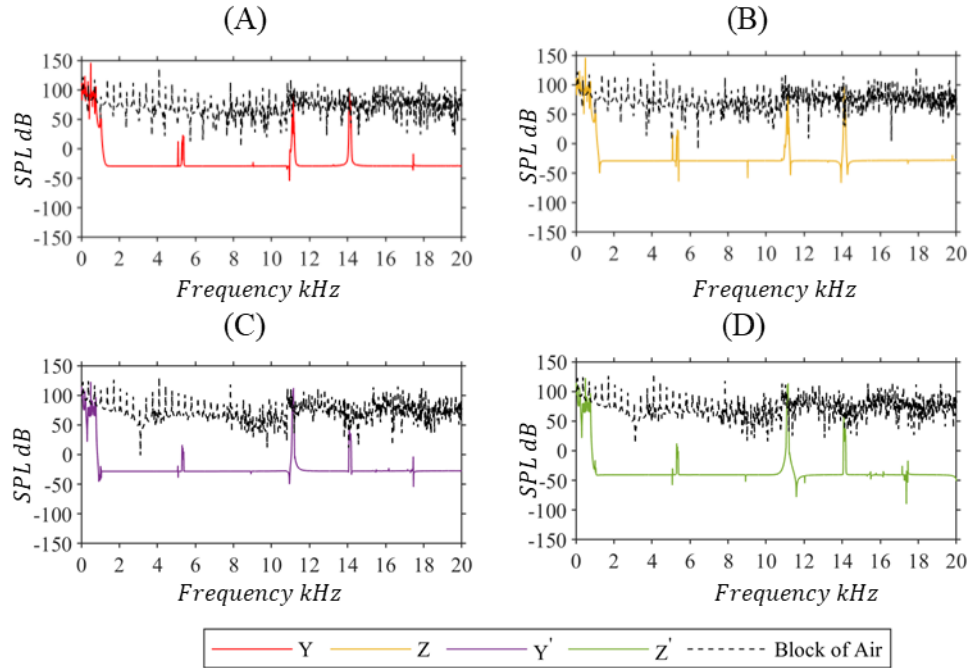


Figure S 5. The acoustic pressure of the other considered sensing locations (i.e., Y,Z,Y',Z') for the 1D acoustic metamaterial made from repeated optimal Tapered-Diverging unit cell.

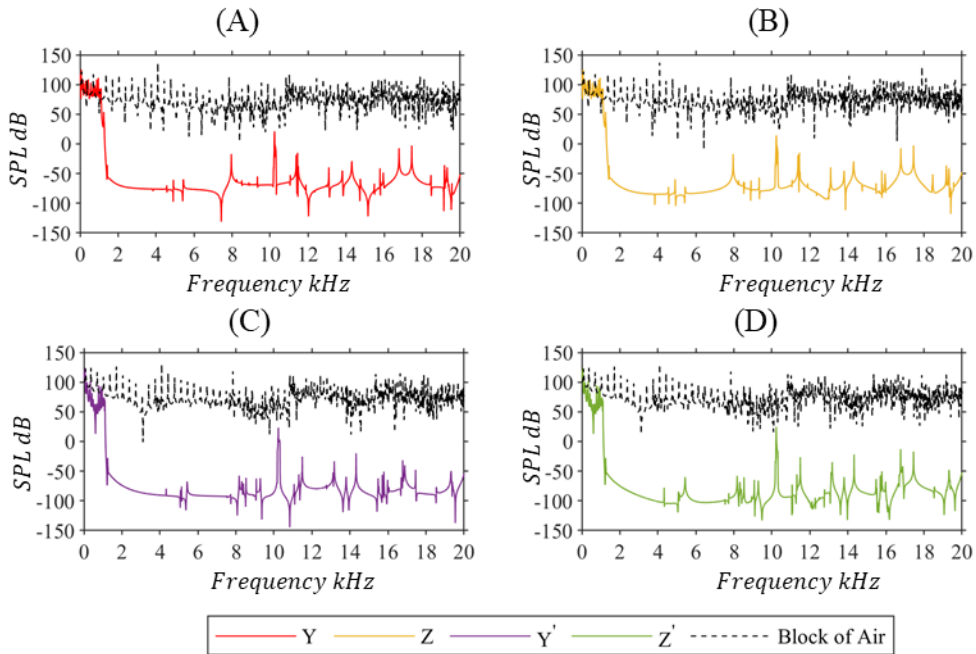


Figure S 6. The acoustic pressure of the other considered sensing locations (i.e., Y,Z,Y',Z') for the 1D acoustic metamaterial made from repeated optimal Tapered-Converging unit cell.

References

1. Shendy, M.; Alkhader, M.; Abu-Nabah, B.A.; Jaradat, M.A.; Venkatesh, T.A. Machine Learning Assisted Approach to Design Lattice Materials with Prescribed Band Gap Characteristics. *European Journal of Mechanics - A/Solids* **2023**, *102*, 105125, doi:10.1016/j.euromechsol.2023.105125.
2. Kushwaha, M.S.; Halevi, P.; Dobrzynski, L.; Djafari-Rouhani, B. Acoustic Band Structure of Periodic Elastic Composites. *Phys Rev Lett* **1993**, *71*, 2022–2025, doi:10.1103/PhysRevLett.71.2022.
3. Sigalas, M.; Economou, E.N. Band Structure of Elastic Waves in Two Dimensional Systems. *Solid State Commun* **1993**, *86*, 141–143, doi:https://doi.org/10.1016/0038-1098(93)90888-T.
4. Liu, Z.; Zhang, X.; Mao, Y.; Zhu, Y.Y.; Yang, Z.; Chan, C.T.; Sheng, P. Locally Resonant Sonic Materials. *Science (1979)* **2000**, *289*, 1734–1736, doi:10.1126/science.289.5485.1734.
5. Elmadih, W.; Chronopoulos, D.; Zhu, J. Metamaterials for Simultaneous Acoustic and Elastic Bandgaps. *Sci Rep* **2021**, *11*, doi:10.1038/s41598-021-94053-3.
6. Bilal, O.R.; Ballagi, D.; Daraio, C. Architected Lattices for Simultaneous Broadband Attenuation of Airborne Sound and Mechanical Vibrations in All Directions. *Phys Rev Appl* **2018**, *10*, doi:10.1103/PhysRevApplied.10.054060.